NRAO Summer Student Lecture Series: ~~1980~~ 1979

Galactic Masers : Observations by John M. Benson

A. Introduction

In 1963, Sander Weinreb made the first successful radio observation of an interstellar molecular transition. He detected OH (hydroxyl) in absorption against the background of the strong continuum radio source Cassiopeia-A. Since then radio astronomers have discovered over 36 molecular species in cool, interstellar clouds. During the late 1960's, anomalously strong and narrow emission lines were being detected at the microwave OH ground-state rotational transitions ($^2\pi_{3/2}$, J = 3/2). While surveying the OH galactic distribution in absorption against backgrounds of HII regions, Weaver and his Berkeley group found the anomalous OH emission toward Orion-A, W3, W51 and W75 (Weaver et al. 1965). Weaver saw strong emission at the $^2\pi_{3/2}$ J = 3/2, F = 1 → 1 and F = 2 → 2 (1665.401 MHz and 1667.543 MHz) OH transitions but little or none at the F = 1 → 2 (1612.231 MHz) transition. The intensity ratios between transitions did not follow the 1:5:9:1 ratio predicted for emission from an optically thin gas nor the 1:1:1:1 ratio for an optically thick gas. The very narrow line widths were consistent with a gas in thermal equilibrium at a kinetic temperature ≤ 50°K. Strong linear polarization was observed in the anamolous 'mysterium' spectrum toward the

HII region W3 (Weinreb et al. 1965). Further observations detected right-handed-circular (RHC) and left-handed-circular (LHC) polarized emission lines at W3 (Davis et al. 1966). With the NRAO 140 ft. radio telescope, Barrett and Rogers (1966) set upper limits on the emission region angular diameter (< 5 arcmin) and calculated an equivalent blackbody brightness temperature of $T_B \geq 2000$°K. Realizing the inconsistency of the high brightness temperature with the low kinetic temperatures required by the narrow line widths, and the anomalous intensity ratios observed by Weaver, Barrett and Rodgers suggested that the anomalous emissions were in fact a result of maser amplification. Subsequent interferometric measurements (Rogers et al. 1966; Cudaback et al. 1966) revealed emission region angular diameters < 20 arcsec. The characteristics of brightness temperatures (> $2(10)^6$°K), polarization, and anomalous transition intensity ratios suggested a celestial maser amplification process (Litvak 1966). Litvak's model maintained the maser transition population inversion by ultraviolet photon pumping.

Three requirements must be met in order to produce amplification by stimulated emission. One, there must be a source of energy not in thermal equilibrium with the masering gas that has enough energy to substantially overpopulate the upper level of the maser transition. Second, there must be a sufficient population of the maser molecular species such that the maser amplification can reach large values. Third, mass motions in the interstellar cloud maser

material must be less than the thermal Doppler line width of the maser transition along the direction of maser gain. The intensity of a beam of radiation propagating through a gas which satisfies the above conditions will increase exponentially with distance. At the point where the amplified beam intensity stimulates emission at a rate exceeding the maser pump rate, the maser amplification becomes linear and the maser is said to be saturated. If I_o is the input intensity to the maser from a background source and the maser is unsaturated, the maser output intensity (Moran 1976) is

$$I(\ell) = I_o e^{\alpha_o \ell} + \frac{\epsilon}{\alpha_o}(e^{\alpha_o \ell} - 1)$$

where ℓ is the propagation path length, α_o contains terms describing the population inversion, pumping rate and transition thermal line width and ϵ/α_o is the source function. The gain of the unsaturated maser is $\alpha_o \ell$ and the amplification $e^{\alpha_o \ell}$. At $\ell = \ell_s$ the maser saturates, $I = I_s$, subsequently $I(\ell)$ becomes (Moran 1976)

$$I(\ell) = (I_s + \frac{\epsilon}{\alpha_o})\alpha_o \ell'$$

where $\ell' = \ell - \ell_s$. While unsaturated, maser amplification narrows the natural transition line widths $\Delta\nu = \Delta\nu_D(\alpha_o \ell)^{-1/2}$, $\Delta\nu_D$ is the

transition thermal Doppler width, $2(\nu/c)(kT/m^{1/2}$. Perturbations in the pumping rate and molecular densities or turbulent motions along the radiation propagation direction have large effects in the output intensity of an unsaturated maser. Thus different maser transitions emanating from the same region of an interstellar cloud can have quite different spectral appearances. For masers saturated over long path lengths, the linear gain begins to dominate. The emission line profiles broaden to the thermal Doppler widths and spectra observed in different molecular transitions take on the appearance of optically thick emissions, that is, similarly appearing spectral structure and intensity ratios consistent with Boltzman population ratios (Fix 1978).

Astrophysical maser gains are typically 20-30, hence providing amplifications of 10^9 - 10^{13}. A maser gain variation of 0.1% results in maser amplification variations of 2-3%.

Hydroxyl is a diatomic molecule with a low moment of inertia and as such has a rotational energy spectrum with transitions in the far-infrared. In the ground rotational state, the electronic orbital angular momentum, $\Lambda\hbar$ is $\hbar$ as $\Lambda = 1$. The angular momentum of the two nuclei rotating as a rigid body is $N\hbar = 0$. The total angular momentum including electronic spin ($\Sigma\hbar$) then is $J\hbar = (\Lambda + N \pm \Sigma)\hbar$. J can take on the sequence of values 3/2, 5/2, 7/2 . . . or 1/2, 3/2, 5/2, 7/2 . . . for (+) and (-) $\Sigma = 1/2$, respectively. When $\Lambda = 1$, the molecule is represented in the $^2\Pi$ state. Each rotational

level is split into Λ-doublets due to slightly different rotational energies when the electronic orbital angular momentum is aligned in opposite internuclear directions. In addition, each Λ-doubled component is split by the proton-electronic angular momentum hyperfine interaction. The total rotational energy quantum number is $F = J \pm 1/2$. Rotational energy levels of astrophysical interest are shown in Figure 1. Note the Λ-doublets have opposite parity. The OH transitions between the ground-state hyperfine quartet ($^2\Pi_{3/2}$ J = 3/2) are those discovered in interstellar clouds during the late 1960's and are generally the most intense OH celestial masers. Ground-state hyperfine transitions of $\Delta F = 0$ ($F = 1 \rightarrow 1$, $F = 2 \rightarrow 2$) are referred to as the main lines and those of $\Delta F = \pm 1$ ($F = 1 \rightarrow 2$, $F = 2 \rightarrow 1$) the satellite lines. The respective frequencies are 1665.40 MHz, 1667.358 MHz, 1612.231 MHz and 1720.533 MHz. In the presence of a small magnetic field B, the energy levels are split into 3 (F = 1) and 5 (F = 2) Zeeman sublevels. The energy offset of the m_F Zeeman sublevel from the B = 0 energy is $\Delta E_F = B\mu_B g_F m_F$, where μ_B is the Bohr magneton, m_F the magnetic quantum number and g_F the splitting factor. The OH ground-state splitting factors are $g_F = 0.701$ (F = 2) and $g_F = 1.169$ (F = 1) for (+) parity. The splitting factors are ~ 0.1% greater in the case of (-) parity. A circularly polarized Zeeman doublet ($\Delta m_F = \pm 1$) is typically split by 0.3 to 1.6 kHz - mG^{-1}.

As of this writing over 250 celestial OH maser sources, 81 H_2O masers, ~ 100 SiO masers and one methyl alcohol (CH_3OH) maser have been detected. Raimond and Eliasson (1967) determined that the position of the Orion-A OH maser is coincident with an infrared (IR) hot spot (± 3 arcsec). They postulated that the OH was being formed in a contracting dust cloud surrounding a warm protostar. Subsequent position measurements by many observers of known OH masers and searches for OH masers toward IR sources cataloged in the C.I.T. 2.2 μm Survey (Neugebauer et al. 1969) have determined that approximately half of all celestial masers are radiating in warm circumstellar dust clouds ($100°K < T < 1500°K$) surrounding evolved M-type giant and supergiant stars. The central stars are for the most part long-period Mira variables and in a few cases irregularly variable supergiant stars.

Stellar OH masers generally develop around cool evolved stars ($T_{surface} \simeq 2000 - 3000°K$) with low surface gravities. There is considerable mass loss resulting in the circumstellar condensation of refractory silicate grains (diameter ~ 0.1 μm), which are subsequently accelerated due to the radiation pressure of the central star. The grain momentum is coupled to the circumstellar gas by collisions, which sweeps the gas outward. The circumstellar dust absorbs the stellar flux and reradiates with a characteristic temperature 1200°K to 250°K. This results in strong IR radiation. Current pumping models for the OH masers favor IR absorption

(Elitzur et al. 1976; Elitzur 1978) over UV absorption or collisional pumps.

Position measurements of maser sources first made by Mezger et al. (1967) and later by many others, have shown OH and H_2O stimulated emission in the immediate vicinity of compact (< 0.5 pc) HII regions excited by very young, UV luminous OB-type stars. The OH masers probably exist in the compressed region between the shock and ionization fronts of the expanding HII regions. These compact HII regions generally occur in regions of multiple star formation, deep in large (10 - 100 pc), cold molecular clouds.

In 1970, Turner instituted a classification system for OH maser sources based on the relative strengths of the quartet of the ground rotational state. Sources exhibiting strong main line emission are classified Type I, those with predominant satellite emissions Type II. Type II is further categorized into IIa (1720 MHz strongest) and IIb (1612 MHz strongest). In the majority of OH sources, either the 1665/7 MHz or 1612 MHz predominates, so classification is relatively unambiguous. His categorization was farsighted as subsequent observations of the OH/IR stellar masers revealed them to be almost exclusively Type IIb and the HII region OH masers Type I. Very few Type Ia (1720 MHz) OH emissions are observed.

B. Late-Type Stars

The gross properties of circumstellar regions surrounding OH/IR stars are shown in Figures 2 and 3. Figure 2 shows a supergiant with high luminosity and low surface temperature undergoing mass loss into a stellar wind. The inner radius of the circumstellar envelope is more uncertain than the outer radius. The basic regimes of the SiO, H_2O and OH masers are indicated. The OH molecules are formed by interstellar UV photons penetrating the dust cloud and photodissociating the H_2O molecules created in the inner, warm regions by the dust grains collisionally dissociating the H_2O molecules (Goldreich et al. 1976). The expansion velocities versus radial distance have been taken from theoretical models by Kwok (1975). The dust temperatures are estimates by Herbig (1970) for the case of VY CMa. More recently calculations by Menietti and Fix (1978) indicate lower dust temperatures.

Long maser path lengths of large gain depend on the gradient of cloud expansion velocities projected along the direction of propagation. For the case of constant radial expansion, Figure 3 shows that the maximum maser amplification toward the observer is

directed along the line of sight to the central star, cases A and B. Maser gains with increasing observer-star impact parameters are substantially less due to the gradient in the projected velocities. This simple model can explain the double-peaked emission spectra that are the definitive signature of OH/IR stars at 1612 MHz. The radial velocity of the star relative to the observer is midway between the red-shifted maser velocity ($V_{star} + V_{exp}$) and the blue-shifted maser velocity ($V_{star} - V_{exp}$), see the spectrum in Figure 3.

The general phenomenological picture of OH/IR stars to date follows.

1. The Central Star

The central stars in identified OH/IR sources are always long-period Mira variables (LPV's) of spectral type M2 - M10 or supergiant, semiregular or irregular variables M3 and later.[1] They are oxygen rich (O/C > 1), have cool photospheres (1500°K < T < 3000°K), are highly luminous (10^4 to $4\ 10^5\ L_\odot$) and undergoing mass loss at rates of $\dot{M} \simeq 5(10)^{-7}$ to $5(10)^{-4}\ M_\odot\ yr^{-1}$. Their highly reddened appearance is due to the thermal IR radiation of the circumstellar dust.

The LPV OH/IR stars have optical periods > 300 days, ages of 10^8 to $5(10)^8$ years, masses $\geq 2.5\ M_\odot$ and apparently are rare (~ 1%) in the overall Mira population (Bowers 1978). The OH/IR LPV's have

[1] The supergiant IRC + 10420 with a spectral classification of F8 Ia is a notable exception.

visual variations of ~ 6 magnitudes as opposed to 2.5 to 8.0 magnitudes for non-OH/IR Miras. The supergiant OH/IR stars comprise < 10% of the M-type supergiants (Bowers 1975).

Large-scale sky surveys of OH/IR stars indicate increasing source densities toward the galactic center and clustering at the leading edges of spiral arms. Bowers (1978) finds the overall galactic distribution of the OH/IR stars to be similar to young objects such as HII regions, supernova remnants and CO molecular clouds but with greater heights above the galactic plane ($\sigma_z \simeq$ 110 pc) and broader velocity dispersions ($\geq$ 30 km s^{-1}). The large galactic scale heights and velocity dispersions suggest that OH/IR stars are among the oldest objects in the 5 - 7 kpc galactic region (Bowers 1978).

There are three distinctive categories of optical spectral features in OH/IR stars (Wallerstein 1975). First, the so-called photospheric absorptions are observed from excited states of neutral Ca, Na, Fe and Ti in the visual-red region (6000 Å to 9000 Å). Second, emission lines requiring low-excitation temperatures (< 3500°K) are seen from H, SiI, FeII, MgI, and TiII. The emission lines may originate in front of velocity shocks in the stellar atmosphere. Third, weak ground-state absorption by CrI and MnI may be influenced by the circumstellar material. Such features are referred to as the circumstellar lines. Wallerstein (1975, 1977) has conducted observations of the Doppler-shifted radial velocities

of the optical features toward the LPV and supergiant OH/IR stars. Wallerstein finds that the circumstellar absorption lines and the emission lines usually have radial velocities near the blue-shifted 1612 MHz OH feature. The photospheric absorption lines are sometimes seen near the stellar radial velocity (midpoint between the double-peaked 1612 MHz OH maser spectra), but are more often red-shifted somewhat randomly toward and beyond the red OH 1612 MHz feature. A detailed interpretation of the exact locations and conditions of the optical emission and absorption regions is unclear to date.

2. The Excess IR Emission

OH/IR stars exhibit large IR excesses for $\lambda \geq 3$ μm. The current hypothesis is that the IR emission is the thermalized and re-radiated stellar flux, which has been absorbed by the circumstellar dust. The shape of the far-IR spectrum indicates that the cloud is not emitting as a blackbody with a unique temperature, rather that the dust temperature decreases from the inner radius ($T \simeq 1500°K$) to outer radius ($T \simeq 300°K$). Typical color indexes are (0.8 μm - 2.2 μm) > 4 magnitudes and (3.5 μm - 10 μm) = 1.4 to 1.4 magnitudes. The I - K index (0.8 μm - 2.2 μm) is linearly correlated with the LPV period (Dickinson et al. 1975). The IR spectra of some OH/IR stars exhibit a 10 μm 'bump', most likely produced by dirty silicate particles (Jones and Merrill 1976; Menietti and Fix

1978). Absorption bands of H_2O and CO at 1.9 μm and 4.7 μm are sometimes present.

3. Maser Intensities and Radial Velocity Structure

The OH maser spectra of OH/IR stars can be divided into three phenomenological categories. The first is from Type I OH/IR stars, which are Mira variables with strong 1665/7 MHz masers and commonly exhibit H_2O masers. The Type I stars show no 10 μm IR excess. The second is from Type IIb LPV OH/IR sources, where the 1612 MHz is strongest. The spectrum is double-peaked with a velocity separation of 5 to 30 km s^{-1}. No preference has been observed for a consistently stronger feature. Dickinson et al. (1975) observe linear correlation of the peak velocity separation with the stellar period. The third is from Type IIb supergiants which are also double-peaked at 1612 MHz but with a greater velocity separation (30 to 60 km s^{-1}). The features are broader than those of the LPV's and the blue-shifted complex of masers is often more intense than the red-shifted features.. Maser emission from the excited rotational states of OH has only been observed toward the giant NML Cyg and must be regarded as a phenomena of the Type I HII region OH masers (Zuckerman et al. 1975).

H_2O masers are commonly detected in OH/IR stars having strong 1665/7 MHz OH emission, usually Type I and Type IIb supergiants. Six cases of double-peaked H_2O masers have been observed in LPV's where the H_2O maser velocities lie interior to the 1612 MHz OH

velocities. In the remaining 50 OH/H_2O/IR sources, the H_2O velocities are near or slightly blue-shifted from the stellar radial velocity.

Maser emission has been observed from rotational transitions of vibrationally excited SiO (v = 1, J = 2 → 1, 86.24 GHz; v = 1, J = 1 → 0, 43.12 GHz) toward OH/H_2O/IR stars (Kaifu et al. 1975; Synder and Buhl 1975). The SiO radial velocities are near the stellar and H_2O maser velocities and always interior to the OH double-peaked velocities. Reid and Dickinson (1976) and Dickinson et al. (1978) have observed broad thermal emission lines in the SiO ground vibrational state from 15 OH/IR stars. The SiO emission peaks midway between the OH double-peaked spectra. Both authors conclude that the stellar radial velocities are centrally located in the OH spectra.

4. Polarization Properties of the Maser Emission

The 1665 MHz and 1667 MHz OH transitions characteristically exhibit strong circularly and linear polarization (up to 100%) while the 1612 MHz features are almost always weakly polarized (< 20%) (Sullivan et al. 1976). In a few rare cases, RHC and LHC Zeeman doublets have been identified in VLBI maps. But for the most part, main line polarized features show little correspondence between opposite senses of circular polarization. To date, linearly polarized features have not been discovered as often as circular features, but this is possibly a selection effect due to observer

preferences for RHC and LHC observations. H_2O masers are weakly linearly polarized (< 10%) if at all, and no polarization measurements have been reported for the SiO masers.

5. Time Variations in the Maser Emission

Variations in the integrated flux densities of the OH 1612 MHz emissions are roughly periodic and in phase with the IR variations from LPV OH/IR stars (Harvey et al. 1974a). Harvey further observes that the OH variation amplitudes are proportional to the length of the IR pulsation period (typically 300 to 800 days). However, no such correlation with IR intensity is observed in main line OH variations. Rather the 1665/7 MHz OH emissions fluctuate in a random fashion over time scales as short as several months. Usually individual main line maser features from the same OH/IR star exhibit independent variations in intensity and polarization. Individual H_2O maser lines apparently change in intensity in the same random manner as the main line OH. However, to date, no efforts have been reported of a comprehensive monitoring program of either H_2O or SiO masers.

6. The Angular Distribution of Maser Emission Features

Three Very Long Baseline Interferometry observations have been made of a sample of LPV OH/IR stars having brightest 1612 MHz OH masers (Reid et al. 1975, 1977; Moran et al. 1977, Benson et al. 1979, Benson and Mutel 1979, Bowers et al. 1980). Two categories of angular structure have emerged. One, those OH/IR stars

with distinct individual maser features spatially distributed in a cloud-like formation. Two, those OH/IR stars exhibiting a core-halo effect in the total angular brightness distribution. The halo could be a smooth, homogeneous maser region or a highly complex array of small maser components blended by insufficient interferometer resolution. Typical maser core sizes are ≤ 0.03 arcsec with $T_B \geq 10^9$°K, and halos ≥ 0.5 arcsec with $T_B \leq 10^8$°K (Reid et al. 1977).

Several recent VLBI observations indicate the OH/IR supergiants have individual maser features typically < 100 AU in extent (Reid et al. 1975, 1977, 1978; Moran et al. 1977; Mutel et al. 1978). The brightness temperatures of such masers are typically 10^9 to 10^{11}°K. Maps of the relative positions of the supergiant 1612 MHz masers reveal cloud-like structure over 1000 to 3000 AU. The red- and blue-shifted feature positions tend to be segregated with the blue features centrally clustered and the red features toward the periphery of the clouds. The overall maser clouds of these supergiants suggests an elongation consistent with a disk rather than a spherical cloud. The total power spectra, representative cross-correlation spectra and maser maps of two supergiant OH/IR stars are shown in figures 4, 5 and 6.

7. Optically Unidentified Type II OH/IR Sources.

Systematic OH surveys of the galactic plane have been conducted by various groups in recent years (Baud et al. 1979 and references therein). Approximately 100 OH/IR objects have been identified as Mira type variables, while 200 OH maser sources (mostly Type II) remain optically unidentified. The unidentifieds show the double-line spectra that are characteristic of Mira type variables. The distributions of the unidentifieds with galactic latitude and longitude, and velocity indicate that they are typically at greater distances from the sun than those OH/IR objects detected optically. Bowers (1978) finds the unidentifieds concentrated in the inner regions of the galaxy with a density peak at 4 to 6 kpc from the galactic center.

Recently the space densities of Type I and Type II OH/IR stars have been better determined. Nguyen-Q-Rieu et al. 1979 and Olnon et al. 1979 conducted searches for OH and H 0 emission using higher sensitivities than previously availiable. They found : a) that Type II luminosities (10^{17} to $5 \cdot 10^{18}$ W) are greater than Type I luminosities ($5 \cdot 10^{15}$ - $5 \cdot 10^{17}$ W), b) most OH/IR Miras within 1 kpc of the sun are Type I, the space density of Type II's is less than that of the Type I's, c) the higher rate of detecting H 0 masers in Type I than Type II OH/IR stars is a selection effect due to the fact that the H 0 masers are typically weak and therefore seen only in nearby Type I sources. Thus, it seems that the unidentified population may be similar to the Type II objects (Miras) we observe nearby.

C. Masers and Young Stellar Objects

Hydroxyl and water masers are generally found in the vicinity of complexes of HII emission and are often spatially coincident with very compact HII regions and IR hot spots. These regions are believed to be in the early stages of the formation of O and B type stars. The OH masers in such regions are predominantly Type I sources. Overall, these regions of star formation may exhibit giant HII regions due to the previous generation of OB stars, and a scattered group of compact HII regions (diameter $\lesssim 1$ pc.), masers and IR sources abutting a dense, cool molecular cloud.

Briefly, the sequential formation of OB stars in associations is as follows. Large dense molecular clouds have been shown to be gravitationally stable, hence external sources of energy are necessary to trigger collapsing regions and subsequent protostar condensations. The initial compression of the neutral molecular material may be the result of shock waves from nearby supernovae or propagating galactic spiral density waves. Star formation is triggered in the outer cloud boundary where that layer collapses under the external shock. If a layer of OB stars form in this region, they will subsequently produce ionization-shock fronts that will drive further into the molecular cloud, thus triggering a new generation of star formation. As well, the OB stars will form an extended HII blister on the cloud surface. After several cycles of sequential star formation, one would observe the original OB association in clear view separated from the molecular cloud. The expanding HII region will have disrupted the remaining local molecular cloud fragments, leaving visible extended remnants of the HII region excited by the OB stars.

Whether or not this scenerio is always the case, the strong H O (in fact, often spectacular) and Type I OH masers direct our attention to those regions where protostars are in the later stages of condensation and are reaching the main-sequence. The spatial and spectral structure of the masers, the detection or not of very compact HII regions and IR sources are signposts indicating different stages of protostellar evolution.

Typical parameters of masers found in the vicinity of young stellar objects are shown in Table II. The H O and OH masers near YSO's are generally more luminous than those in the circumstellar shells of evolved, late-type giant stars.

1. OH Masers

The OH masers are predominantly Type I with the i665 MHz usually a factor of two stronger than the 1667 MHz. Often 1612 MHz and 1720 MHz emission is detectable, although it is always weaker than the main-line emission. The Type I OH masers are spectrally complex and spread over a velocity range ~ 20 km s^{-1}; they are typically highly circularly polarized and exhibit intensity variations on time scales of months. When properly identified, Zeeman split features consistantly indicate magnetic field strengths ~ 10 milligauss. Such a field strength is consistant with $n_H \sim 10^6$ cm^{-3}, where the magnetic field lines were frozen in to regions condensing from typical interstellar densities, $n_H \sim 1$ cm^{-3}, and magnetic field strengths 1 microgauss. Recent observations with high degrees of spatial and flux sensitivities are finding that the OH masers are coincident with very compact HII regions. Thus the compact HII regions are probably a necessary condition for maser action.

With the developement of VLBI mapping software and the expansion of the VLB Network, mapping of maser features has reached a certain tentative maturity. Adaquate uv coverage and accurate interferometer amplitude and phase calibrations now allow applying the aperture synthesis mapping technique to masers. The results of two such experiments are currently availiable for comment.

Reid et al. (1980) observed the 1665 MHz W3(OH) OH masers with an 8 element VLBI array. They detected and mapped 70 distinct maser components in front of a bright HII region. The masers appear in about a dozen isolated clusters, see figure 7 . Assuming that the velocity spread in each cluster is due to Zeeman splitting, Reid et al. (1980) determined that the mean radial velocity for the W3(OH) OH masers is -44.3 km s^{-1} $\pm$ 1.0 km s^{-1} LSR . Molecular emission lines and HII recombination lines are seen at -47 to -50 km s^{-1}, thus the OH masers are red-shifted with respect to the background HII region and are apparently in the remnant accreting material. NH_3, observed in absorption against the HII region, has a velocity of -44.5 km s^{-1} . This further indicates that the OH masers are formed in a collasping cloud external to the HII region.

Benson and Mutel (1980) have observed the 1665 MHz and 1720 MHz OH masers in the W51(Main) region with a 5 element VLBI array. They find the OH masers in two separate regions approximately 6 $(10)^{17}$ cm apart, see figures 8 and 9. Each masing region is coincident with a very compact HII region and near H_2O maser clusters (although not coincident). Currently, accurate velocity information about the HII regions is unavailable. Thus the kinematics of the maser regions is as yet uncertain.

These observations have however shown that individual maser features may not be regarded as symmetrical spots. Rather some features appear complex and elongated (see figure 10) .

2. H_2O Masers

Like the water masers associated with late-type stars, the H_2O masers near young stellar objects exhibit rapid intensity variations (weeks to months) and low levels of polarization. Their spectral and spatial appearance , however, suggests that a degree of catagorization is possible. There are two basic classifications. One, H_2Osources with spectra confined to a narrow velocity range ($\sim$15 km s^{-1}). These low velocity spectra may be simple lines, double lines, triple lines or somewhat more complex. The symmetrical appearance suggests emission regions of ordered kinematic structure. For example, the triple-peaked H_2O spectrum of VY CMa originates in a region of radial expansion. The central peak coming from masers at the stellar velocity and the other two from opposite sides of the expanding cloud. Low velocity maser regions are usually about 10^{16} cm in diameter. Two, some H_2O spectra show features well dispersed in velocity (20 km s^{-1}) from their low velocity features. These high velocity masers are often more variable and weaker than the low velocity emission. The high velocity maser clouds are about $10^{16.5}$ to $10^{17.5}$ cm in diameter.

An example of a young stellar object with low and high velocity H_2O masers is W51(M). Figures 11 and 12 show the W51 spectrum and maser maps (Genzel et al. 1979). Note that most of the low velocity features (55 to 70 km s^{-1}) lie in a core region surrounded by a shell ($\sim 3\ 10^{16}$ cm) of high velocity masers.

Genzel et al. (1979) suggest that W51(M) is a massive, young O star surrounded by a dense, differentially rotating and expanding disk (5 10^{15} to 3 10^{16} cm). The low velocity masers occur in the disk, while the high velocity features are density enhancements driven by a strong stellar wind into the adjacent molecular cloud. The W51 region in figure 11 may be the site of multiple star formation. Each compact HII region and associated OH masers, the W51(M) H_2O complex and the W51(S1) H_2O masers probably represent four sites of stellar evolution, and indeed two or possibly three stages of the star formation process.

OH and H_2O masers, very compact HII regions and IR hot spots are signposts that appear at different stages in the star formation sequence. At this writing, however, there is no clear and unequivocal relationship between the occurance of a particular observational signpost and a distinct stage of stellar evolution. But a pattern has begun to emerge. The earliest stage of a young, stellar object, the pure accretion phase, seems to be accompanied by very long wavelength (1 mm) IR, while the fairly high correlation of OH masers and very compact HII regions certainly indicates that the OH maser phase occurs after the star has reached the main-sequence. The crucial intermediate stages are less clear and more controversial. The H_2O maser spectra with simple velocity only may originate in the accreting material before the central star has achieved enough luminosity to power the strong stellar winds evidenced by the high velocity H_2O masers. Since very compact HII regions are almost never observed coincident with dense H_2O maser clusters, the H_2O maser phase probably indicates that stage of evolution before or at the very beginning of HII formation.

TABLE I.*

Characteristics of Masers Associated with Late-type Stars

Quantity	H_2O	OH	SiO
transitions observed	1	3	5
number known[a]	100	130[b]	60
linewidth (km/s)	1-2	1-2	1-2
$T_K(^oK)$[c]	400-1500	400-1500	250-3500
number of spectral features[d]	1-10	1-10	1-10
velocity range (km/s)	5-50	5-80	2-15
polarization (percent)	none	small	linear (0-50)
lifetime of feature (s)	$>10^7$	$>10^7$	$>10^7$
spot size	10^4	10^{15}	10^{14}
$T_B(^oK)$	10^{11}-10^{12}	10^9-10^{11}	10^{11}
cluster size (cm)	10^{15}	2×10^{15}	10^{14}-10^{15}
power (ergs/s)[e]	10^{24}-10^{28}	10^{24}-10^{28}	10^{26}-10^{27}

a complete list in Engels.[33]

b 145 more sources are known whose spectra resemble those seen towards later-type stars but for which there is no optical or IR object seen, possibly because of obscuration.

c assuming no line narrowing or mass motions.

d more for super giants.

e assuming isotropic radiation. 10^{24} ergs/s is the sensitivity limit for present radio telepscopes for masers at a distance of 100 pc.

TABLE II.*

Characteristics of Masers Associated with Young Stellar Objects

Quantity	H_2O	OH	SiO	CH_3OH
transitions observed	1	9	4	8
number known	170	~100	1[a]	1[b]
linewidth (km/s)	0.5-2	0.1-1	1-2	0.5-2
$T_K(^oK)$[c]	100-1500	5-500	3500	150
number of spectral features	1-200	1-50	~5	~10
velocity range (km/s)	1-400	1-30	25	4
polarization (percent)	linear(0-20)	linear(0-100) circular(0-100)	none	none known
lifetime of feature[d] (s)	10^6-10^8	10^7-10^8	$>10^7$	$>10^7$
spot size (cm)	10^{13}-10^{14}	10^{14}-10^{15}	10^{14}	$\sim10^{16}$
$T_B(^oK)$	10^{13}-10^{15}	10^{12}-10^{13}	10^9	10^3-10^4
cluster size (cm)	10^{16}-10^{17}	10^{16}-10^{17}	$<10^{15}$	3×10^{17}
power[e] (ergs/s)	10^{25}-10^{33}	10^{25}-10^{30}	10^{29}	10^{28}

a the only source known is in Orion A. The classification of the SiO maser is controversial.

b the only source known is in Orion A.

c assuming no line narrowing or mass motions.

d there are some cases of shorter time scales.

e assuming isotropic radiation. 10^{25} ergs/s is the sensitivity limit for present radio telescopes for masers at a distance of 300 parsecs.

* FROM 'MASER ACTION IN NATURE', J.M. MORAN, CFA PREPRINT # 1304, 1980.

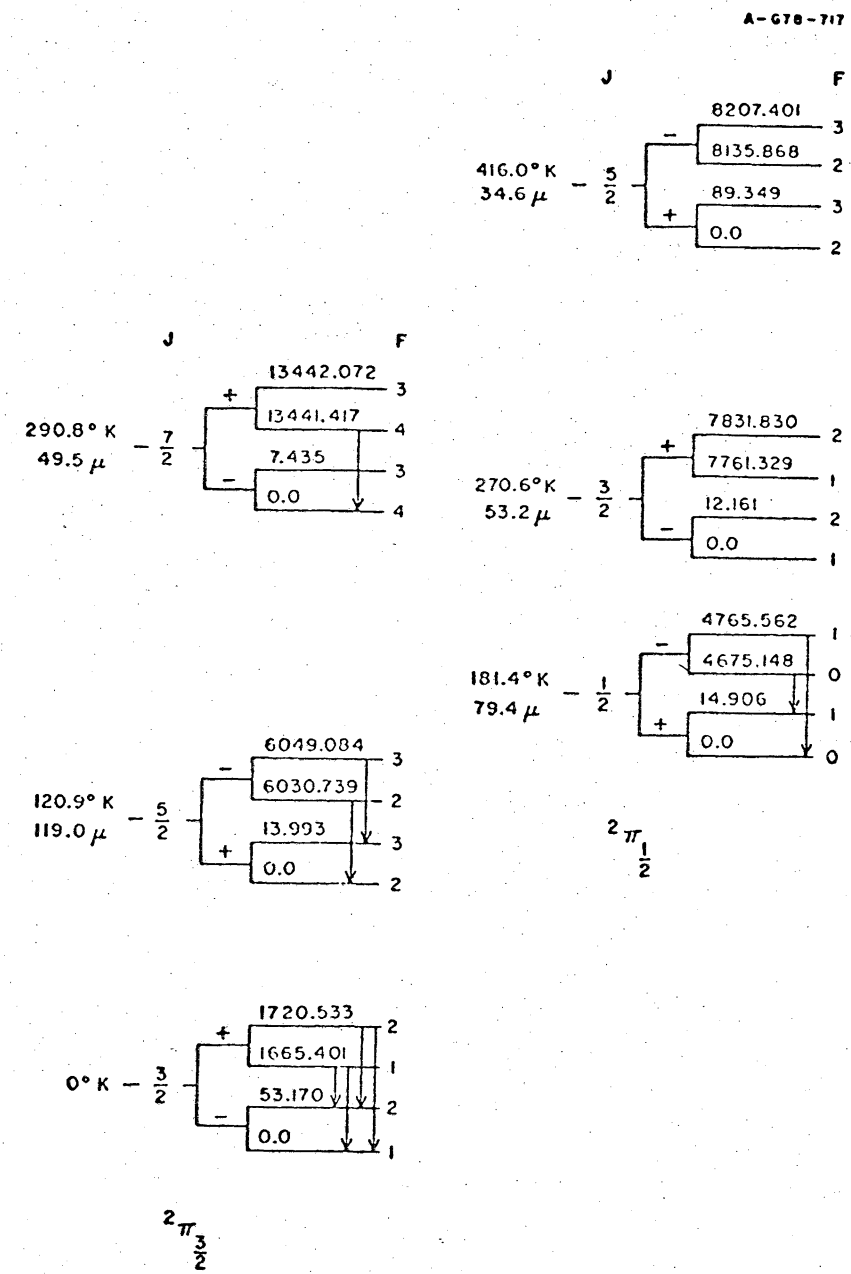

Figure 1. Rotationally excited states of the OH molecule split by Λ-doubling and hyperfine interaction into quartets of levels (not to scale). The hyperfine splitting is indicated in units of 10^6 Hz. Observed celestial maser transitions are shown.

C-G78-781

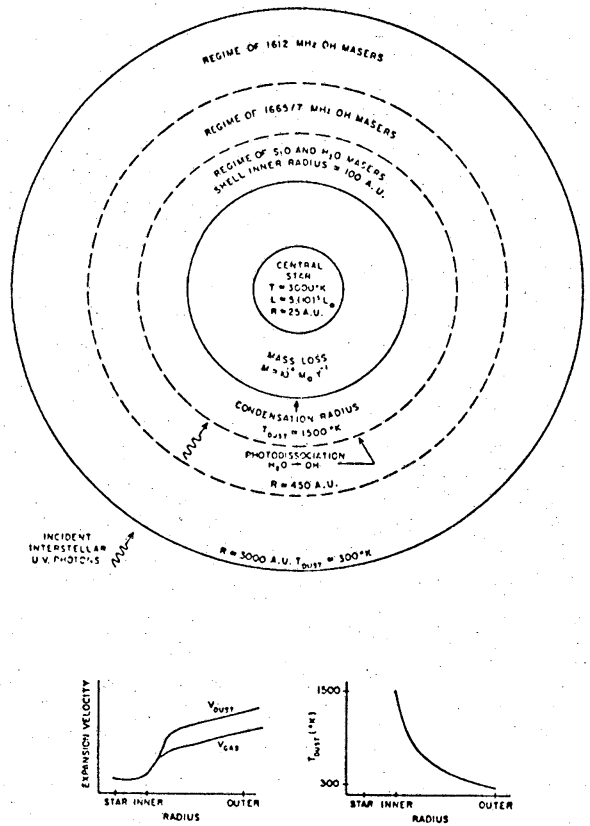

Figure 2. The morphology of an expanding circumstellar shell surrounding a cool supergiant star. The regions of molecular species emitting maser emission are shown. This figure is not drawn to scale. The expansion velocities and temperature profile are plotted with increasing radial distance within the shell.

B-G78-780

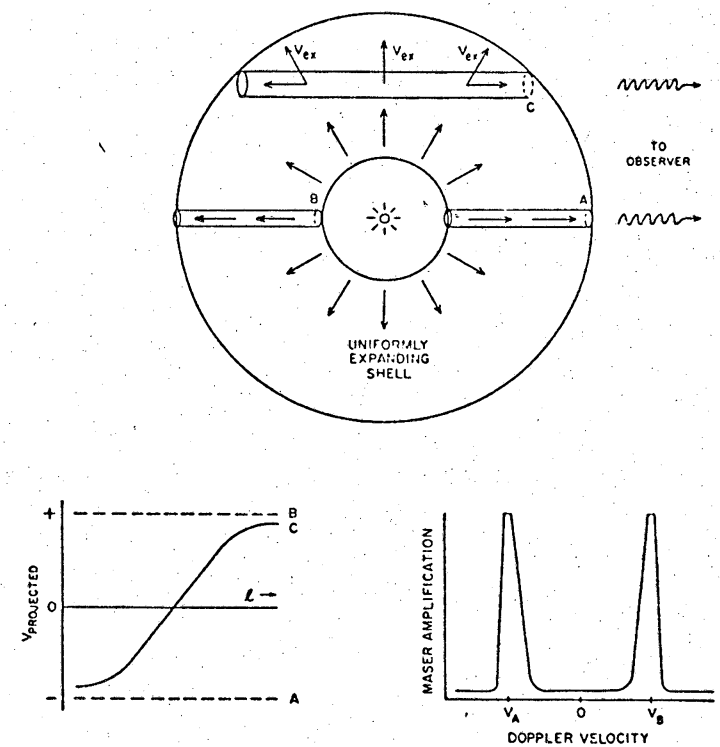

Figure 3. Maser emission in a uniformly expanding circumstellar shell. Three possible maser tubes are shown (A, B and C). The expansion velocity projected onto the observer's line of sight with distance along each maser tube is shown in the lower left graph. For resonant masers ($\Delta V/V_{ex} \ll 1$) amplification by stimulated emission occurs over the entire lengths in masers A and B, whereas the resonant path length in maser C is very short. In the case of unsaturated masers, amplification increases exponentially with ℓ and a double-peaked emission spectrum is observed (lower right).

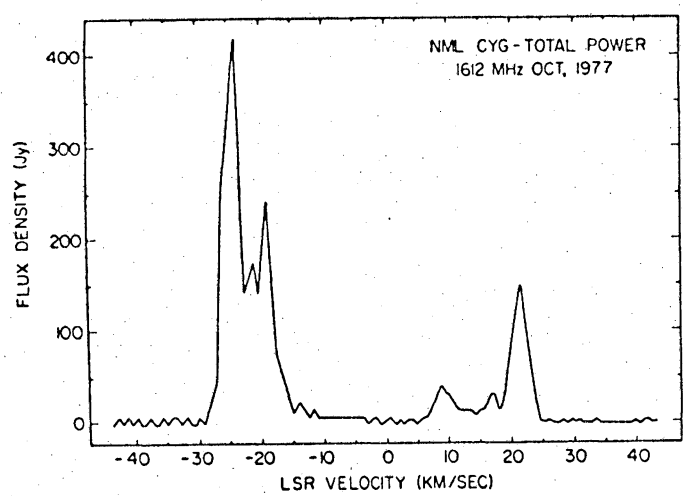
NML CYG - TOTAL POWER
1612 MHz OCT, 1977
FLUX DENSITY (Jy)
LSR VELOCITY (KM/SEC)

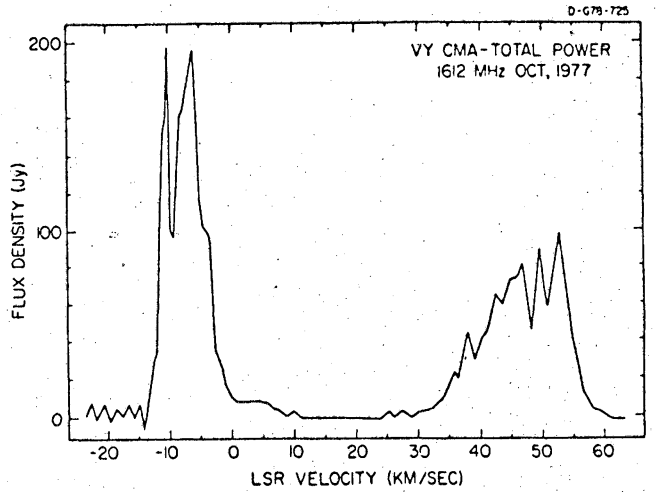
D-G78-725
VY CMA - TOTAL POWER
1612 MHz OCT, 1977
FLUX DENSITY (Jy)
LSR VELOCITY (KM/SEC)

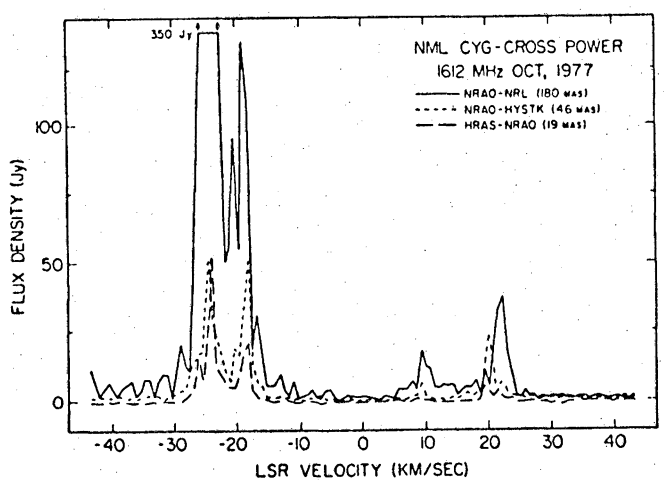
350 Jy
NML CYG - CROSS POWER
1612 MHz OCT, 1977
NRAO-NRL (180 MAS)
NRAO-HYSTK (46 MAS)
HRAS-NRAO (19 MAS)
FLUX DENSITY (Jy)
LSR VELOCITY (KM/SEC)

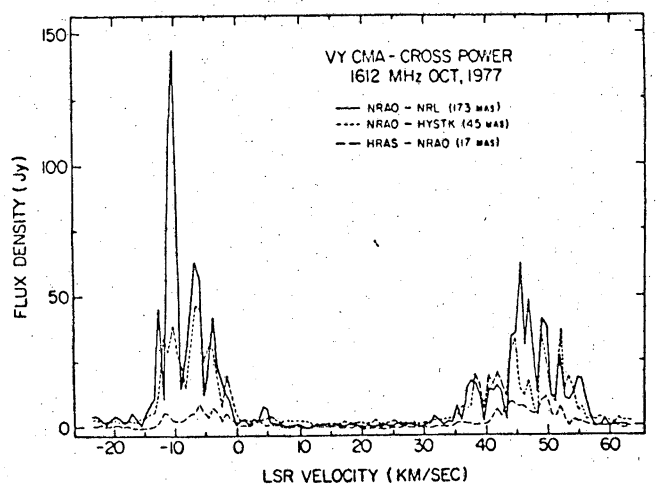
VY CMA - CROSS POWER
1612 MHz OCT, 1977
NRAO - NRL (173 MAS)
NRAO - HYSTK (45 MAS)
HRAS - NRAO (17 MAS)
FLUX DENSITY (Jy)
LSR VELOCITY (KM/SEC)

FIGURE 4

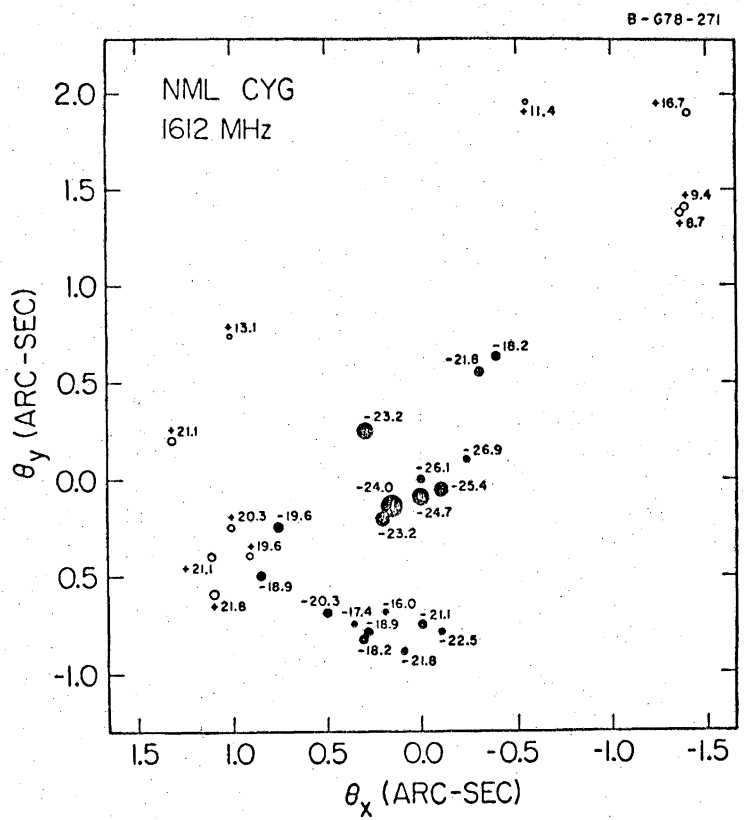

FIGURE 5.

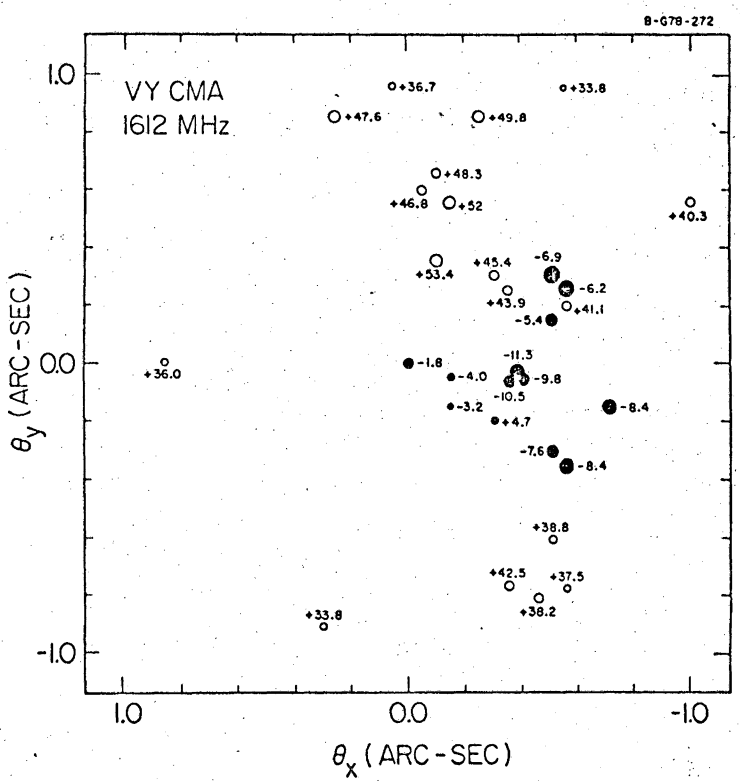

FIGURE 6.

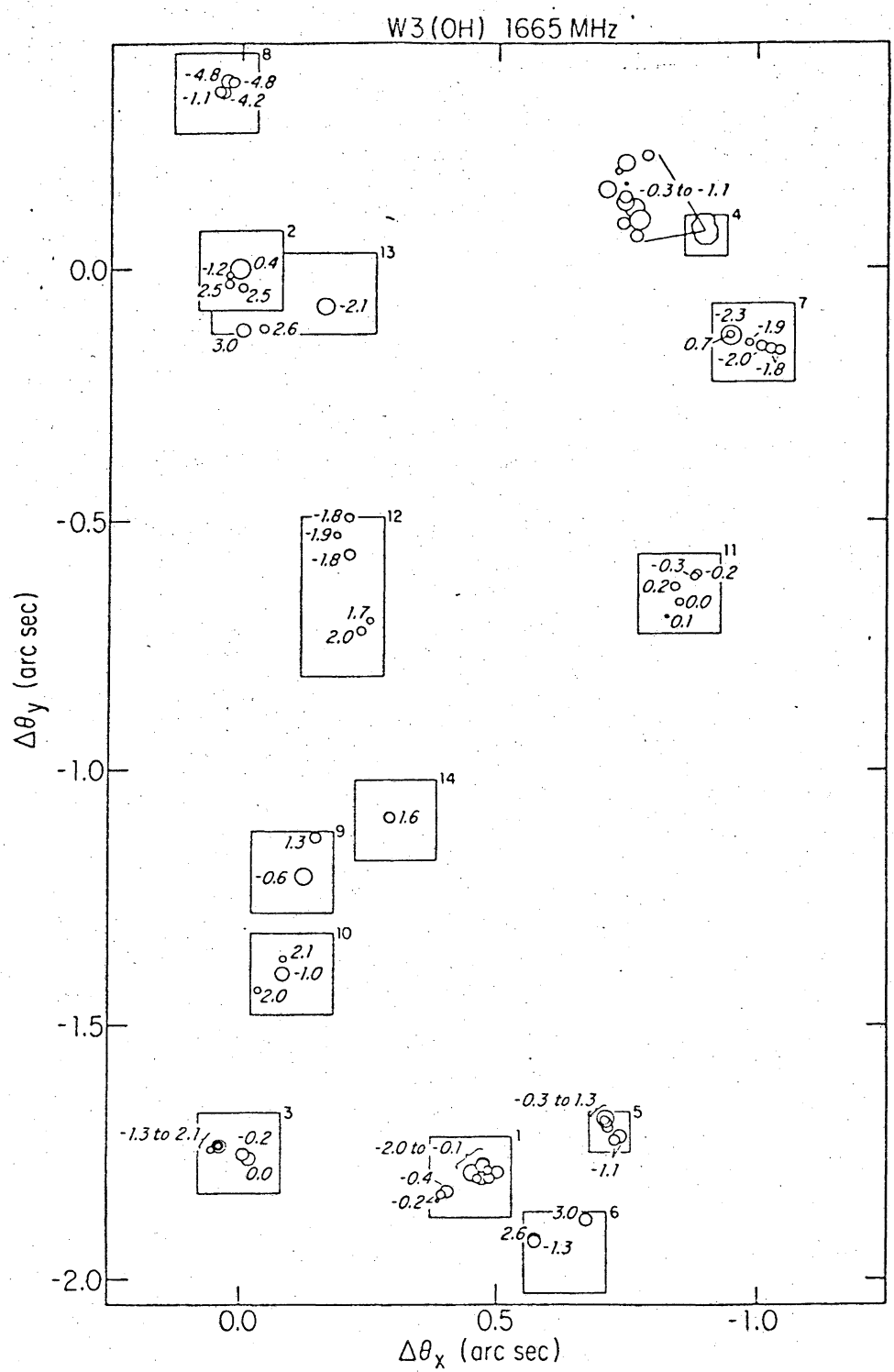

Figure 7.--A spot map of the OH maser emission from W3(OH). Each circle corresponds to a maser component listed in Table II. The size of each circle is proportional to the logarithm of the peak brightness temperature of the maser. A radial velocity, v, is indicated next to the circles and is the LSR velocity offset from -44.3 km s^{-1} (i.e., v_{LSR} + V -44.3). This map was constructed from spectral-line synthesis maps from 14 regions indicated by the boxes (typically 0".16 on a side); the number of the map region is above the upper right hand corner of the box and corresponds to the map region in Table II. The reference feature used to define the origin of the map has v_{LSR} = -43.9 km s^{-1}. The absolute position of the origin of the map is R.A. (1950) = $02^h23^m16^s.46$ ($\pm 0^s.01$) and Dec.(1950) = $61^\circ38'57''.8$ ($\pm 0''.1$). θ_x and θ_y are angular offsets on the sky toward the east and north, respectively.

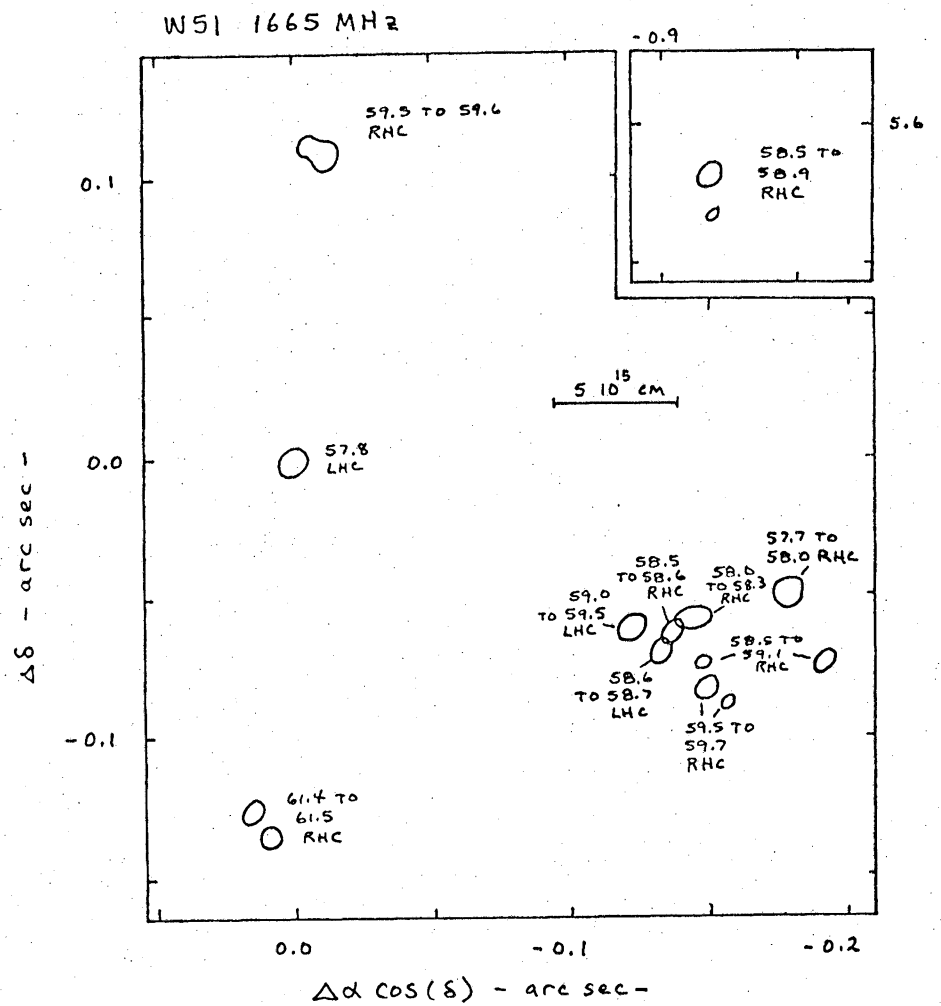

FIGURE 8

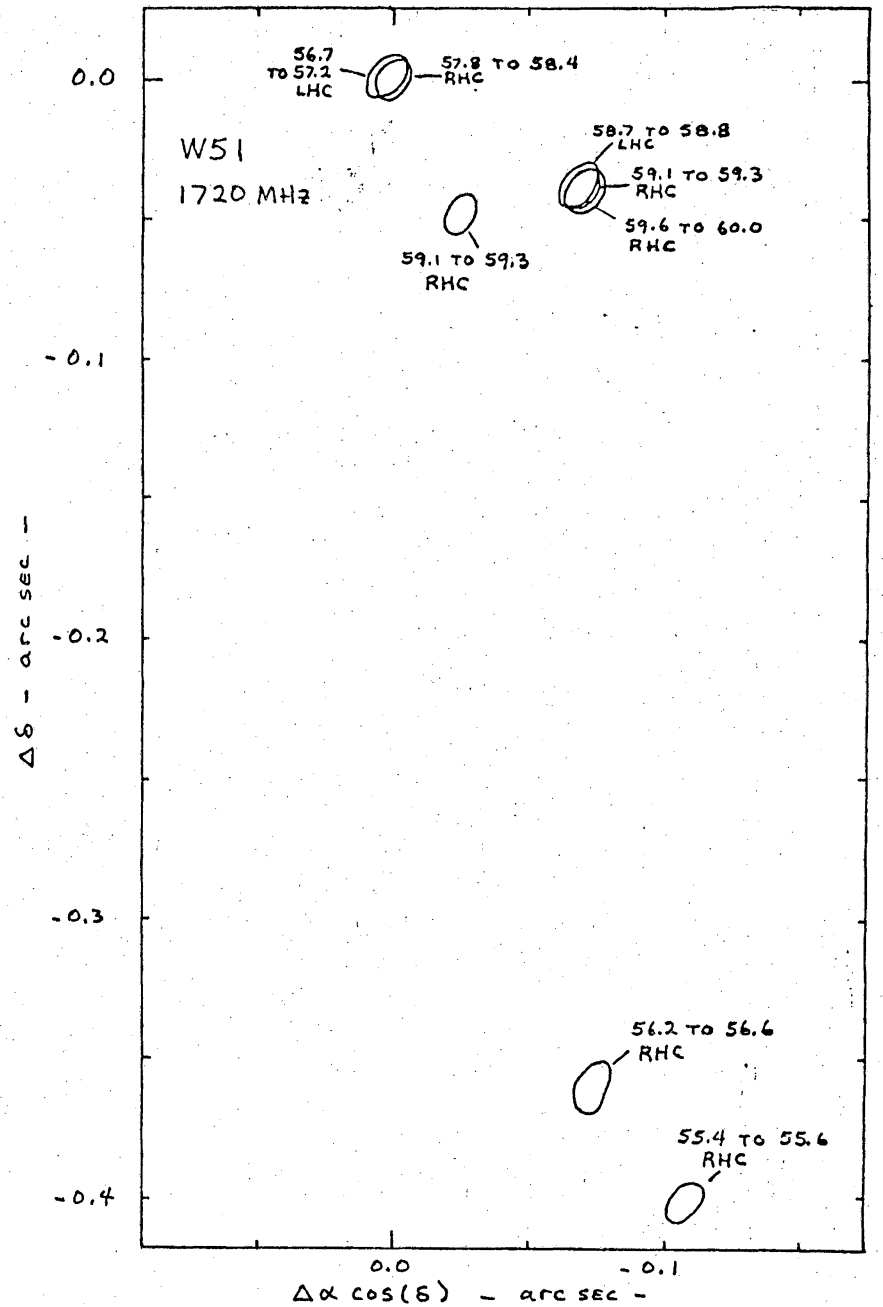

FIGURE 9

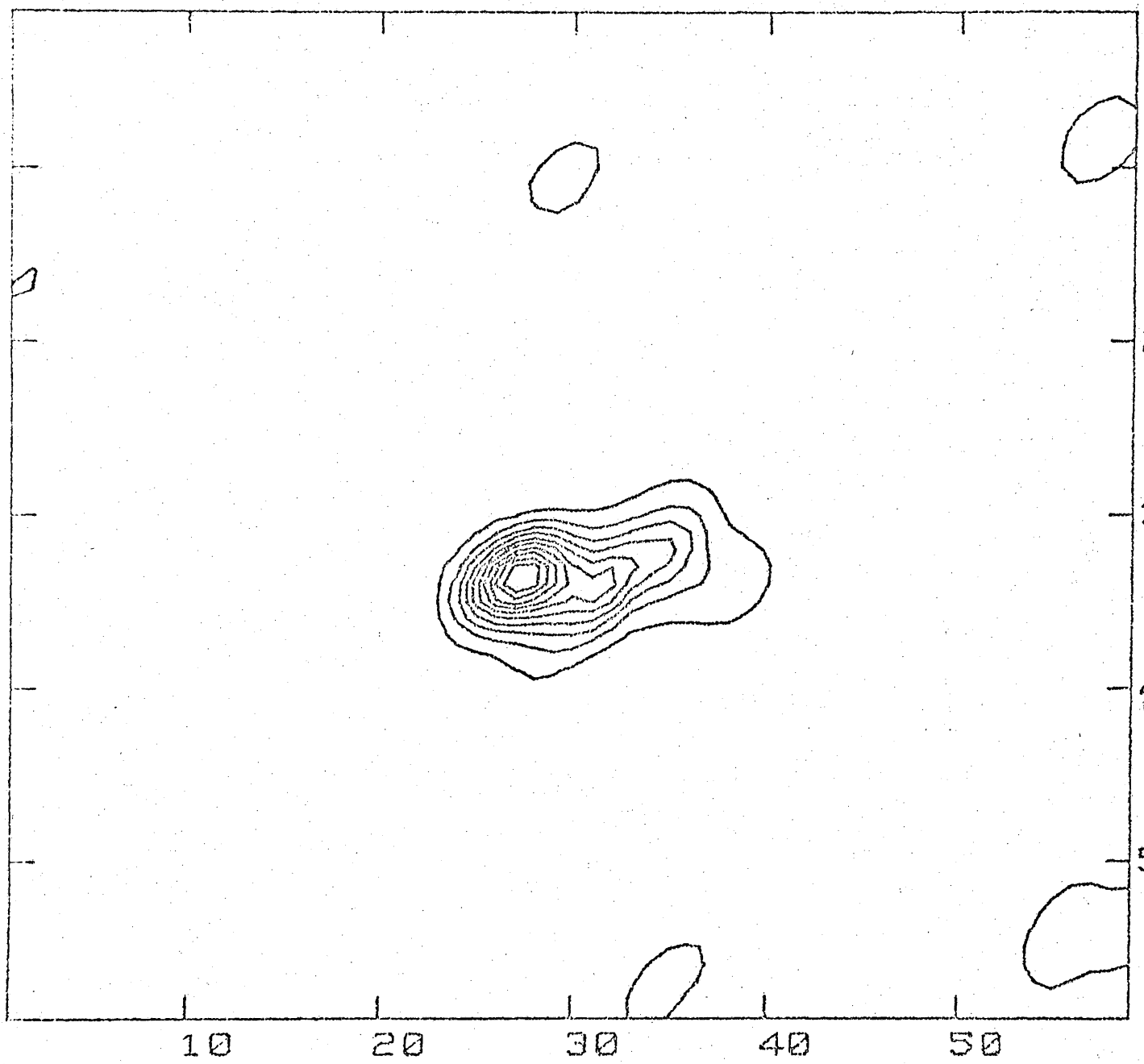

28/4

FIGURE 10

α = 19 21 26.2 ± 0.02
δ = 14 24 43.6 ± 0.4
{H_2O REF}

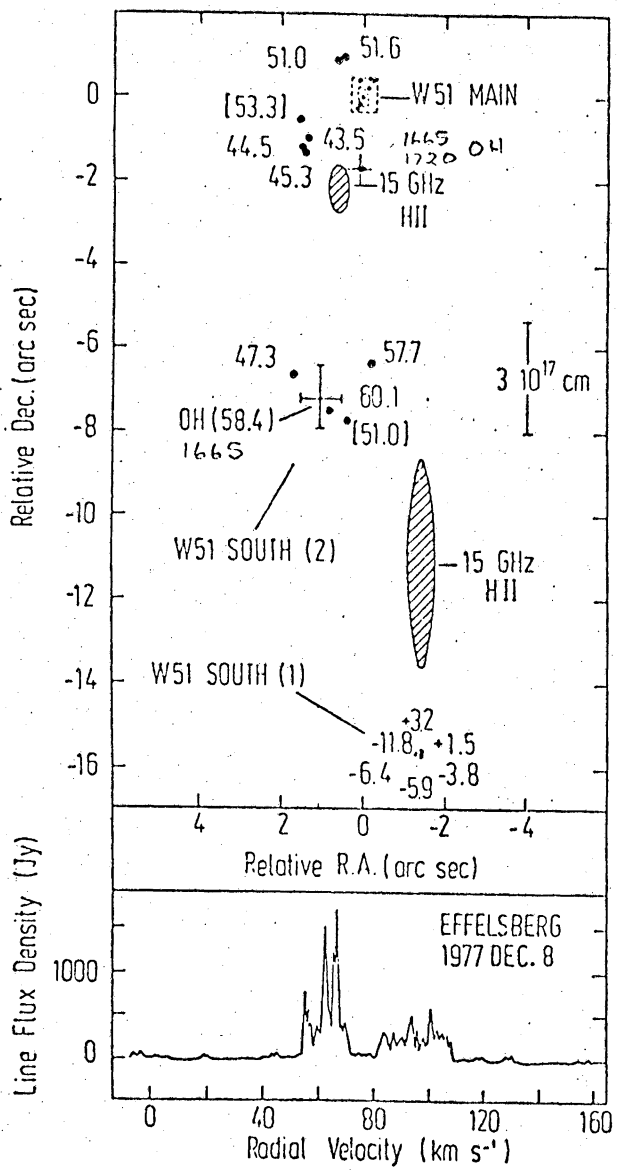

Figure 11

FIG. 1

Wynn-Williams OH 1665
α = 19 21 26.3 ± 0.2
δ = 14 24 35 ± 3
.7 km s⁻¹ resolution

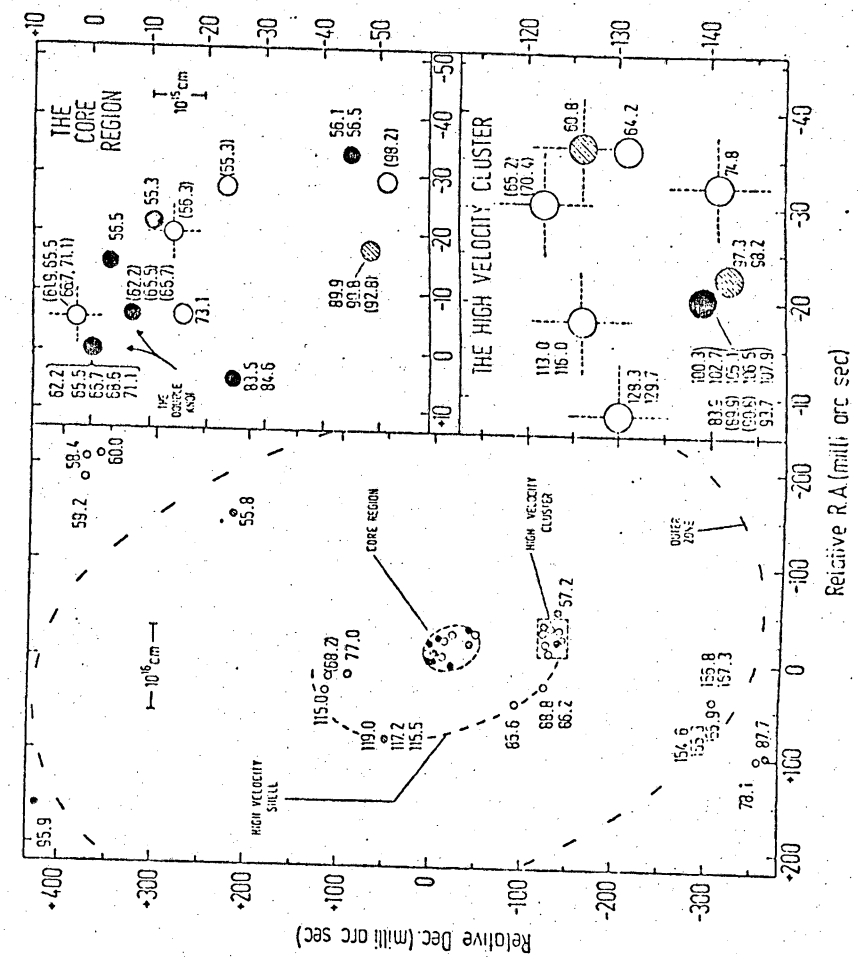

$\Delta\theta_x$ = -0.9
$\Delta\theta_y$ = +5.6
OH OFFSET

Figure 12.

FIG. 2